Dynamical complexity response in Traveling Ionospheric Disturbances across Eastern Africa sector during geomagnetic storm using Neural Network Entropy

Oludehinwa[1], I. A., Velichko[2], A., Ogunsua[3,4], B.O., Olusola[1], O.I., Odeyemi[1], O.O., Njah[1], A.N., Ologun[4], O.T.

1. Department of physics, University of Lagos, Lagos, Nigeria.
2. Institute of Physics and Technology, Petrozavodsk State University, 31 Lenina Str., 185910 Petrozavodsk, Russia.
3. Key Laboratory for middle Atmospheric and Global Environment Observation (LAGEO), Institute of Atmospheric Physics (IAP), Chinese Academy of Science, Beijing, China.
4. Department of physics, Federal University of Technology, Akure, Nigeria.

Abstract

This paper examines the response of dynamical complexity in Traveling Ionospheric Disturbances (TIDs) across Eastern Africa sector during 2015 major geomagnetic storms. Detrended Total Electron Content (DTEC) derived from Eight stations of Global Positioning System (GPS) receivers across Eastern Africa was used to unveil the transient features of dynamical complexity response in TIDs. Neural Network Entropy (NNetEn) was applied to the detrended TEC time series data to capture the degree of dynamical complexity. The NNetEn track the distinct features associated with the occurrence of TIDs. As the signatures of TIDs begin to emerge, we found low values of NNetEn signifying reduction in the degree of dynamical complexity response as TIDs occur while high values of NNetEn were depicted as the signatures of TIDs subsides signifying increase in the dynamical complexity response, as the

TIDs signatures begin to subsides. Also, we found that the response of dynamical complexity associated with TIDs features expands from the Southern Hemisphere and diminishes at the Northern Hemisphere. Reduction in dynamical complexity response associated with the occurrence of TIDs is more evident in the Southern Hemisphere compared to Northern Hemisphere indicating that the propagation of TIDs is more prominent in the Southern Hemisphere. Furthermore, we found that the propagation of TIDs is more prominent at Equinoctial season compared to solstitial season. The latitudinal observation of NNetEn revealed higher degree of dynamical complexity response in ADIS and NEGE signifying that the development of TIDs is minimal in ADIS and NEGE. Finally, the reduction in dynamical complexity associated with the occurrence of TIDs were obvious during all the phases of geomagnetic storms. In particular, the dynamical complexity response at initial and recovery phases of geomagnetic storm depicts more TIDs features.

Keywords: Geomagnetic storm, Traveling Ionospheric Disturbances (TIDs), Neural Network Entropy (NNetEn), Dynamical complexity, Total Electron Content (TEC).

1.0 Introduction

Traveling Ionospheric Disturbances (TIDs) are sudden wave-like propagation irregularities that perturbate the state of the ionospheric plasma. They are usually driven by the propagation of acoustic gravity waves (AGWs) manifested in both the lower and upper atmospheric conditions (Hunsucker, 1987; Hocke and Schlegal, 1996; Ding et al. 2007; Vadas and Liu, 2009; Kelley et al. 2003; Tsurutani et al. 2012; Vadas and Crowley, 2017; Burleigh et al. 2018; Yufei et al. 2021).

In the upper atmosphere, Large-scale Traveling Ionospheric Disturbances (LSTIDs) are generated through the electrodynamics processes of induced energy from the magnetosphere (Richmond and Roble, 1979; Song et al., 2012; Balasis et al. 2019; Ma et al. 2020). Such that during geomagnetic storms, high latitude thermosphere is heated via joule effect, and consequently energy is transferred towards lower latitudes in the form of thermospheric waves that interact with ions in the ionosphere (Fuller-Rowell et al., 1996). Also, equatorward expansion of strong ionospheric irregularities zone and enhancement in the field-aligned currents drives a simultaneous intensification of LSTIDs occurrence (Cherniak and Zakharenkova, 2018).

Meteorological/geological events such as thunderstorm, sudden stratospheric warming, Volcanos, tsunamis, underground nuclear explosion, typhoon, earthquakes propagate Medium-scale Traveling Ionospheric Disturbances (MSTIDs) (Artru et al., 2005; Occhipipinti et al. 2013; de Jesus et al., 2017; Meng et al., 2019b; Jonah et al., 2021; Kundu et al., 2021; Maletckii and Astafyeva, 2021). For instance, findings on thunderstorm have shown that the activities of lighting produced during thunderstorms can transfer energy from the troposphere through gravity waves and infrasonic waves to the region of the ionosphere (Mohannakumar, 2008; Sindelarova et al., 2009; Freeshah et al., 2020; Ogunsua et al., 2020; Borchevkina et al., 2021). These studies have unveiled the connections between the lower atmospheric layers and the ionosphere (troposphere-stratosphere-ionosphere coupling). Notably, both LSTIDs and MSTIDs are often observed during geomagnetically disturbed and quiet periods respectively and can infer a phenomenon where the ionospheric plasma density is reshaped and destabilized thereby pose an operational hazard on radio communication, navigation and imaging system (Nishioka et al., 2013; Azeem et al., 2017).

The rapid fluctuation in Total Electron Content (TEC) is one of the features of TIDs and GPS is commonly used to study the occurrence of TIDs due to its wide spatial coverage compared to other instruments such as ionosondes, High Frequency (HF) Doppler sounder, radio telescopes and incoherent scatter radars. Interestingly, the occurrence of TIDs have been observed in different regions including Africa, Asia, Europe, North America and South America. Song et al. (2012) studied the LSTIDs using the TEC observed from GPS network in the regions of North America, Europe, and East Asia during the 7-10 November 2004. They detected four LSTIDs events in North America, four in Europe and three in East Asia. Also, two new propagation features of LSTIDs were observed. One was the latitudinal dependence of the LSTIDs propagation azimuths that tend to deflect more to west from south as they propagate to low latitudes indicating that the Coriolis force was one of the main causes of the LSTIDs southwestward deviation. The other was the different mean horizontal phase velocities of LSTIDs among different regions indicating that the amplitudes of LSTIDs decreased during their propagation for every event and the daytime damping rates were more than one times larger than the nighttime ones due to different ion drag between daytime and nighttime. Zhang and Tang (2015) examined the evidence of TIDs driven by tsunamis using GPS-TEC in New Zealand. They found TIDs which have similar horizontal velocity and direction as the tsunami waves at different times after the event and recommend that besides the propagation velocity and direction, the arrival time of tsunami is crucial to distinguish tsunami-driven TIDs correctly. Cherniak and Zhakharenkova (2018) investigate the origin, occurrence, and propagation of LSTIDs over the European region during the 2015 December geomagnetic storm. It was found that during the main phase of the geomagnetic storm, the LSTIDs propagates equatorward from European high latitudes to middle latitudes ($35\text{-}40^0$ N) with the horizontal velocities of

approximately 700-800m/s. Liu et al. (2019) studied the LSTIDs in the Asian sector during the 2015 St. Patrick's Day geomagnetic storm. Their findings revealed that an LSTIDs spanning at least 60^0 in longitude (80-140^0E) occurs as a result of possible atmospheric gravity waves (AGWs) propagating from high to lower latitudes at around 09:40-11:40UT and the crest of this LSTIDs shows a tendency of dissipation starting from the eastern side.

Jonah et al. (2020) looked at the inter-hemisphere traveling ionospheric disturbances and their mechanisms. The authors reported a consistent features of higher Ne density and stronger TIDs in the low-latitude Southern Hemisphere (SH) as compared to the Northern Hemisphere (NH). They also found that the meridional component of the neutral wind during geomagnetically disturbed days can play an important role in TIDs. Ferreira et al. (2020) investigate the potential precursors for the TIDs occurrence using detrended Total Electron Content (TEC) derived from 880 ground station of Global Navigation Satellite (GNSS) across Europe sector. They reported that LSTIDs observed are frequent with higher amplitude during the periods of enhanced auroral activity and attributed joule heating due to dissipation of Pederson currents as the main contributor to the excitation of LSTIDs. In addition, they further suggest that LSTIDs are excited predominantly after strong ionosphere perturbation occurred at high latitude. Wen and Jin (2020) applied ground based dual-frequency GPS observations to monitor TIDs during 10th July 2018 Typhoon Maria. They found two significant ionospheric disturbances on the southwest side of the typhoon eye between 10.00 and 12.00 UTC. Both TIDs reached up to 0.2 TECU and the amplitudes were slightly different. Inaddition, their findings confirm that the upward propagation of gravity waves were the main cause of the TIDs during Typhoon Maria. Cheng et al. (2021) used an automatic detection algorithm: Three-dimensional Fast Fourier Transform (3-DFFT) and

support vector machine (SVM) on TEC observation in Taiwan/Japan. To statistically examines the MSTIDs at the low-latitude Equatorial Ionization Anomaly (EIA) region in the Northern Hemisphere. They observed that MSTIDs at southward are found almost every day during 0800-2100LT in spring and winter. At midnight, southward MSTIDs are more discernible in summer and majority of the TIDs are propagating from Japan to Taiwan. In the northward, MSTIDs are more frequently detected around 1200-2100LT in spring and summer.

In Africa sector, Katamzi and Habamlema (2013) investigate the amplitude, periods and virtual propagation characteristic of the storm induced ionospheric disturbances from GPS measurement over South Africa region during geomagnetically disturbed periods of 29-31th October 2003. It was found that a large sudden TEC increase on 28th October, 2003 was noticed, the day before the first of the two major storms investigated. The diurnal trends of TEC and foF2 measurement revealed that the geomagnetic storm caused a negative ionospheric storm such that TEC and foF2 were depleted between 29 and 31 October, 2003. Seun et al. (2020) present the climatology of MSTIDs during geomagnetically quiet days over the North Africa region. They reported that MSTIDs occurrence is a local phenomenon and its occurrence rate is majorly dependent on LT, season and latitude. It was also found that both daytime and night-time MSTIDs over North African is dominantly propagate southward (equator). However, MSTIDs dominantly propagate towards the South-East (SE) during daytime and towards the South-West (SW) during nighttime. Ogunsua et al. (2020) applied the method of polynomial filtering on TEC measured from the equatorial Global Positioning System (GPS) receiver stations along the west Africa region-Congo Basin to examine the significant daytime ionospheric perturbation by thunderstorms. They found that the TEC deviation due to thunderstorm were mostly propagated in a specific direction from the point of the event. Also, it was reported that the internal dynamics of the

equatorial ionosphere was suppressed by large thunderstorm effect at daytime with negligible impact during night.

Despite the huge body of knowledge outlined in the above literatures and the references therein, the idea of traveling ionospheric disturbances have not been investigated from the concept of information theory. The generation of irregularities in the ionosphere is driven by the continuous interactions from the lower and upper atmospheric forcing controlled by the coupling processes of plasma diffusion, $E \times B$ drifts, thermospheric neutral winds, and chemical processes, which are propagated nonlinearly. This nonlinearity emerges when interactions among atmospheric drivers are not directly proportional (Dakos, 2019) and could have a great influence on the complexity and internal dynamics of the ionosphere since all these inherent irregularities can lead to chaotic variation at all geophysical condition (Unnikrishnan, 2010). Notably, the expansion of neutral clouds, the photoionization process and the movement of charged particles bound by magnetic fields introduces instabilities of plasma (Stubbe and Hagfors, 1997; Zhu et al., 2020). Thus, leading to rapid variation in ionospheric electron density that drives the occurrence of TIDs. Interestingly, the underlying dynamics of TIDs exhibits some significant fluctuation signatures that calls for further investigation.

In nonlinear dynamics, the concept of entropy is developed from information theory to measure the degree of disorderliness (irregularities) in a dynamical system. Hence, it describes complexity of the system. With the broaden exposure of Artificial Intelligence (AI) technology in Space Weather applications, Neural Network had been a prominent tool in AI technology. In lieu of this, our present study proposes to examine the Day-to-Day dynamical complexity response in the traveling ionospheric disturbances across Eastern Africa sector during 2015 major geomagnetic storms using Neural Network Entropy (NNetEn). NNetEn is based on

158 classification accuracy by computing entropy directly without considering the probability
159 distribution (Velichko and Heidari, 2021). The model applies a unique algorithm for evaluating
160 the complexity of a time series with every given length. It also has good performance in the time
161 series with some equal values.

162 The Africa equatorial ionosphere possesses high degree of irregularities due to its consistent
163 driving of plasma instabilities (Ogunsua et al., 2020; Arowolo et al., 2020; Bolaji et al., 2022).
164 Therefore, the propagation of TIDs across Eastern Africa sector needs a special attention.
165 Because the Eastern Africa sector is known to exhibit strong structures of Equatorial Ionization
166 Anomaly (EIA) (Joseph et al. 2015; Olwendo et al. 2015; Adebesin et al. 2018; Seba et al. 2018;
167 Oyedokun et al. 2020). This inturn has a strong driving influence on the propagation of TIDs
168 within this sector. The need for additional practical method for investigating and tracing the
169 ionospheric behaviour during TIDs has led to the use of dynamical complexity method such as
170 (Approximate Entropy, Tsallis Entropy, Shannon Entropy, Sample Entropy, Permutation
171 Entropy and Neural Network Entropy) for examing the responses of the ionosphere to TIDs
172 during geomagnetic storms. This framework is inspired from previous works based on TIDs and
173 investigation on the dynamical complexity in the ionosphere. Considering the fact that dynamical
174 complexity has been applied to show ionospheric responses to dynamical changes. In this paper,
175 we have applied NNetEn to trace the effects of TIDs on the dynamics of the ionosphere.
176 Therefore, Artificial Neural Network Entropy (NNetEn) which measures the irregularities of a
177 dynamical system will be employed to study the degree of dynamical complexity response due to
178 TIDs during major geomagnetic storms of 2015. To address the research question, that can
179 NNetEn trace the response of the ionosphere during the emergence of TIDs. Notably, these

observations can be a useful diagnostic in unveiling the features of dynamical changes in the ionosphere as TID emergences.

2.0 Data Acquisition and Method of Analysis

The Eastern Africa is a sub-region of Africa continent. Its climate is rather uncommon of equatorial region due to the region's high altitude and rain shadow of the westerly monsoon wind created by the Rwenzori mountains and Ethiopia Highlands (Dewar and Wallis, 1999). At the ionospheric layer, the signature of acoustic gravity waves in the ionosphere is manifested as oscillations of the ionospheric electron density and the equatorial ionosphere of Africa sector is known to be highly complex. This region exhibits severe ionospheric irregularities due to plasma instabilities driven by fountain effect operations (Kelley, 1989; Kelley et al. 2013; Balasis et al. 2019; Bolaji et al. 2022).

The measurement of Total Electron Content (TEC) from GNSS in Rinex format was obtained from the archive of UNAVCO (https://www.unavco.org) during the months of 2015 major geomagnetic storms to study the traveling ionospheric disturbances (TIDs) within the Eastern region of Africa sector. Notably, the major geomagnetic storms in the year 2015 occurred in March, June and December with intensities of -234nT, -208nT, and -170nT respectively. We choose the GPS stations situated within the Eastern region of Africa sector to unveil the occurrence of TIDs and its nonlinear dynamical characteristics that are associated with March, June and December 2015 major geomagnetic storms. The geographical and geomagnetic location of the GPS stations investigated are shown in Figure (1) and Table 1. The Receiver Independent Exchange (RINEX) format of the GPS receiver was processed using GPS_Gopi_v2.9.9 TEC processing software developed by G.K. Seemala, (2017). Slant TEC were derived from the RINEX data files using an algorithm developed at Boston College, USA which uses phase and

code values for both $L_1(f_1 = 1575.42MHz)$ and $L_2(f_2 = 1227.60MHz)$ GPS frequencies to remove differential clock error effects (Seemala and Valladares, 2011; Nade et al. 2015; Odeyemi et al. 2022).

$$\Delta(\delta t) = \delta t_{L1} - \delta t_{L2} \quad (1)$$

$\Delta(\delta t)$ is the time delay in pseudo-range (∂t_{L1}) at L_1 and pseudo-range (∂t_{L2}) at L_2.

$$\Delta(\delta t) = 40.3 \times TEC \times \frac{(f_{L1}^2 - f_{L2}^2)}{(c \times f_{L1}^2 \times f_{L2}^2)} \quad (2)$$

Where f_{L1} and f_{L2} are the group path lengths corresponding to the high and low GPS frequencies. c is the speed of light in vacuum. Then TEC becomes:

$$TEC = \frac{1}{40.3} \times \frac{(c \times f_{L1}^2 \times f_{L2}^2)}{(f_{L1}^2 - f_{L2}^2)} \times \Delta(\partial t) \quad (3)$$

After obtaining the slant TEC data, the TEC series was subjected to Savitzky-Golay FIR smoothing filter with 5th order polynomial. Savitzky-Golay (S-G) method is effective at preserving the high frequency components of the signal and is based on local least-square polynomial approximation. We refer interested readers to the work of Savitzky and Golay, 1964; Shekhar, 2016; Ostertagova and Ostertag, 2016 for detailed computational procedure. To obtain the signatures of TIDs, the detrended TEC data was obtained by calculating the difference between the S-G fitted values from the TEC values to remove diurnal trend so that the amplitude of the wave perturbation can be determined. Below is the mathematical description of the detrended TEC series derived.

Suppose we have a GPS TEC series in the form

$$X(t) = [x_1, x_2, x_3, \dots, x_i] \quad i = 1,2,3, \dots, 1440 \quad (4)$$

Subjecting $X(t)$ to Savitzky-Golay algorithm, we have

$$P(t) = [X_1, X_2. X_3, \ldots., X_i] \quad i = 1,2,3, \ldots, 1440 \tag{5}$$

The TEC deviation is given as

$$TEC_{dev} = X(t) - P(t) \tag{6}$$

To monitor the global scale of geomagnetic activities, the planetary K_p and A_p index during March, June and December 2015 was archive from the International Services of Geomagnetic Indices (ISGI), https://isgi.unistra.fr. Furthermore, the polar cap North (PCN) and South (PCS) indices were from the IGSI website. While the 1-minute SYM-H was acquired from the National Aeronautics and Space Administration (NASA), Space Physics Facility (https://omniweb.gsfc.nasa.gov/).

2. 1 Calculation of Neural Network Entropy (NNetEn) Measures

NNetEn is an Artificial Neural Network LogNNet model used to estimate the entropy of a time series data. The model was proposed by Velichko and Heidari, 2021 and is based on classification accuracy which computes entropy directly without considering the concept of probability distribution. The method modifies the structure of LogNNet classification model such that the classification accuracy of MNIST-10 digits dataset indicates the degree of complexity of a given time series (Velichko, 2020). The model comprises of two parts (Figure 2). The first part is the reservoir which uses the matrix W_1 by transforming the input vector (Y) into another vector (S_h). In the reservoir part who's their element is constructed from the time series data. We apply the method of row-by-row filling with time series stretching in filling the matrix of the reservoir (W_1). The second part is the Feedforward Neural Network which classify the input

vector (S_h) into digits 0-9 at the output layer (S_{out}). The NNetEn Algorithm estimates the entropy in following steps explained below: Loading of the time series data; Loading MNIST-10 and T-pattern; Initializing Weights; Filling the matrix of the reservoir (W_1); Calculating normalization coefficients; The number of training epochs (*Ep*=1) is set; Training of the LogNNet; The testing process of the LogNNet network is performed and classification accuracy is calculated; NNetEn calculation as

$$NNetEn(Ep) = \frac{Classification\ accuracy}{100\%} \tag{5}$$

The Learning Inertia (LI) is calculated from

$$LI(Ep1/Ep2) = \frac{NNetEn(Ep2) - NNetEn(Ep1)}{NNetEn(Ep2)} \tag{6}$$

Where $Ep1$ and $Ep2$ are the number of epochs used in calculating the entropy (*Ep*1=20, *Ep*2=1).

This parameter can be considered a new characteristic of the input time series, and characterizes the speed of training of a neural network, can be used to identify transient processes in the dynamics of time series.

3.0 Results

Figure 3 shows the time series of TEC observation measured at Addis Ababa on 26th March 2015 depicting the diurnal trend of TEC variation. To unveil the signatures of TIDs, the extracted TEC was subjected to the Savitzky-Golay filter method of detrending. The variation of the detrended TEC time series on 26th March 2015 at Addis Ababa is shown in Figure 4. It was observed that the detrended TEC depicts a compression in the TEC wave pattern with a sudden spike in its underlying dynamics at approximately 0500UT, 0700UT and 1800UT. This sudden

spikes in the amplitude of TEC wave pattern unveils the presence of TIDs on 26th March at Addis Ababa. The detrended TEC observation on 30th March shown in Figure 5 depicts a consistent variation in the TEC wave pattern with no sudden spikes in its underlying dynamics. Thus, signifying the absence of TIDs signatures. Notably, these TIDs are obvious in the detrended TEC in the form of complex fluctuation signatures (i.e sudden spikes in TEC wave pattern) which unveils the nature of spatial and temporal variability in the internal dynamics of the ionosphere. The hidden dynamical information in the detrended TEC as the presence of TIDs signatures emerges is captured using NNetEn to describe the dynamical complexity response of the ionosphere. The transient features of NNetEn as the signatures of TIDs begin to emerge in the detrended TEC at Addis Ababa on 26th of March is depicted in Figure 6. A decline in the NNetEn (20), NNetEn (1) and LI (20/1) values was observed as the presence of TIDs signatures begin to emerge, (see Figure 6a-d). Figure 7 demonstrates absence of decline in the NNetEn (20) and small fluctuation of NNetEn (1) and LI (20/1), which corresponds to the absence of TIDs in the TEC wave pattern at Addis Ababa on 30th of March. We noticed a consistent trend of high values of NNetEn (20) and NNetEn (1) signifying that the absence of TIDs is associated with high values of entropy. As NNetEn (1) more sensitive to TEC wave pattern we use it for NNetEn evaluation.

To observe the geomagnetic activity driven by the changes in the interplanetary magnetic field, solar wind and the geoffectiveness of interplanetary electric field. We display in Figure 8, the global scale of day-to-day geomagnetic activities during the March 2015 geomagnetic storm. It was observed that most of the days depicts $K_p \leq 3$ signifying the consistent occurrence of interplanetary disturbances in the dynamics of the magnetosphere for most of the days in March 2015. Notably, the highest values of planetary indices $K_p \approx 8$ and $A_p \approx 180$ was depicted on the

17th of March. Inaddition, the Polar Cap South (PCS) and Polar Cap North (PCN) indices also depicts high value $\sim 12 mV/m$ unveiling an enhancement in interplanetary electric field as the main phase of the geomagnetic storm emerge. The day-to-day geomagnetic activities unveils the level of interplanetary disturbances associated with the emergence of TIDs during the month of March 2015 and we notice that there is a consistence occurrence of interplanetary disturbance in the day-to-day geomagnetic activities in the upper atmosphere which can be attributed to Equatorial factor (Arowolo et al. 2020; Bolaji et al. 2022).

In Figure 9, we display the day-to-day latitudinal plot of NNetEn distribution across Eastern Africa sector during the month of March 2015. We observed a reduction in the values of NNetEn as the presence of TIDs signatures begins to emerge in the detrended TEC. As the signatures of TIDs in the detrended TEC begins to subsides, the values of NNetEn increases. These reductions in NNetEn as TIDs emerges were depicted in blue colour while the enhancement in NNetEn as the signatures of TIDs begins to subsides are depicted in green, brown and yellow colour. Interestingly, we found that the spread of blue colour in the latitudinal plot of NNetEn unveils the distribution of TIDs across the Eastern Africa sector during the day-to-day ionospheric dynamics in the month of March 2015. Notably, this indication of blue colour associated with the emergence of TIDs is noticed to spread from the Southern Hemisphere (SH) and diminishes at the Northern Hemisphere (NH). In some occasion, the distribution of TIDs unveils by the NNetEn spreads up to the Northern Hemisphere. These interesting features were obvious on the 3rd, 16th-17th, 22nd and 28th of March 2015. We further noticed a reduction in the day-to-day NNetEn observation in most of the daily ionospheric dynamics at MOIU. NNetEn values depicted at DODM and MBEY revealed a drastic reduction in most of the day-to-day observation. In addition, we found that the values of NNetEn at MTVE, KASM and MZUZ on

26th-31st are very low, because the latitudinal plot was seen to depict blue colour during these periods. High values of NNetEn were evident at NEGE and ADIS in most of the daily observation. We also noticed that on the day of major geomagnetic storm (17th March 2015), the NNetEn unveils some traces of low values of entropy from MZUZ to ADIS, this is an indication that the ionospheric disturbances created due to 17th of March 2015 geomagnetic storm travels up to the Northern Hemisphere.

Figure 10 depicts the global scale of the day-to-day geomagnetic activities during June 2015 geomagnetic storm. On the 22nd of June, the day of the main phase of geomagnetic storm, the K_p and A_p was ~ 7 and 200 respectively. The Polar Cap index was $\sim 12 mV/m$ during the main phase depicts high values of electric fields. Interestingly, most of the day-to-day observation of K_p index revealed $K_p \geq 2$ except on 22nd of June where the K_p is 8. These indexes signify that level of day-to-day interplanetary disturbances in the upper atmosphere in the month of June 2015 is moderate.

Displayed in Figure 11 is the Latitudinal plot of NNetEn distribution from Ethiopia to Malawi during the month of June 2015. We noticed that the features of low entropy associated with the emergence of TIDs is minimal compared to the day-to-day latitudinal NNetEn observation in March 2015. The highest value of NNetEn were depicted at NEGE and ADIS signifying that the propagation of TIDs in these regions is minimal during the month of June 2015. However, traces of low values of NNetEn were obvious in MOIU, DODM and MBEY on 1st-5th, 7th-16th, 22nd-30th of June 2015 signifying the emergence of TIDs in the observed station. At KASM and MZUZ, high values of NNetEn were observed in most of the days. However, on the 22nd June, the day of the major geomagnetic storm, we notice the features of low values of NNetEn

spreading from MZUZ to MOIU. Similar features of NNetEn were also observed on 23rd-25th of June.

The global scale of day-to-day geomagnetic activities during the month of December 2015 is shown in Figure 12. The day of the main phase of geomagnetic storm (20th June) depicts $K_p \geq 6$ and $A_p \sim 100$. However, most of the day-to-day K_p values were found between 2 and 4. Inaddition, high values of polar cap index ($\sim 10 mV/m$) was also observed on the 20th of December 2015. The day-to-day latitudinal observation of NNetEn distribution across the Eastern Africa during the month of December 2015 is shown in Figure 13. We found that the NNetEn unveils high values of entropy in ADIS, NEGE, MOIU, KASM and MZUZ for most of the day-to-day observation. It was further noticed that high values of NNetEn associated with the absence or no TIDs is evident in all the stations. This observation strengthened the evidence that during the month of December, the development of TIDs in the Eastern region of Africa sector is minor. Interestingly, on the 1st-2nd, 8th-10th, 16th and 20th December, (a day of major geomagnetic storm), we found some features of low NNetEn values especially at MOIU signifying some mild features of TIDs.

3.1 Latitudinal observation of dynamical complexity during initial, main and recovery phases of 2015 major geomagnetic storm

We display in Figure 14, the features of NNetEn distribution during different phases (initial, main and recovery) of major geomagnetic storm in March 2015. It was noticed that the emergence of TIDs associated with the traces of reduction in NNetEn were depicted during all the phases of the storm. Notably, this traces of reduction in NNetEn were found to be pronounced around 15-21UT. Furthermore, drastic reduction in NNetEn were more prominent

during the initial and recovery phases compared to the main phase. This observation unveils the idea that the Eastern African ionosphere could develop the propagation of TIDs due to the coupling processes of plasma diffusion, $E \times B$ drifts, and thermospheric neutral winds (Kelley, 2013). We suspect that the electrodynamics processes in the thermosphere could generate gravity waves with neutral winds strong enough to influence the propagation of TIDs during initial, main and recovery phases of geomagnetic storm.

In Figure 15, the phases of June 2015 geomagnetic storm revealed high values of NNetEn at initial, main and recovery phases with slight evidence of reduction in NNetEn during the main phase indicating that the propagation of TIDs due to the initiation of initial and recovery phases of the storm is minimal during the June 2015. The lowest values of NNetEn seen during the main phase was evident at DODM. Finally, the latitudinal plot of NNetEn distribution at initial, main and recovery phases of December 2015 shown in Figure 16 revealed high values of NNetEn during all the phases. However, traces of slight reduction in NNetEn during the main phase were observed compared to the initial and recovery phases.

4.0 Discussion of the Results

The sudden spikes of wave pattern in the TEC variation exhibits nonlinear signatures that includes frequent drift and amplitude enhancement in wave pattern. It's influence on the internal dynamics of the ionosphere could lead to chaotic variation due to inherent irregularities driven by plasma instabilities (Kelley, 1989; Fejer et al., 1999; Kelley et al., 2003). Notably, these irregularities possess high degree of nonlinearity features in its underlying dynamics that can be captured through information theory (Oludehinwa et al. 2018). The degree of

disorderliness/irregularities in a dynamical system is defined by the entropy measures and thus describes its dynamical complexity. Notably, the underlying dynamics of the ionosphere as a dynamical system depends on the changes in external influences and its various internal irregularities leading to chaotic behaviour and dynamical complexity (Unnikrishnan et al. 2006; Unnikrishnan and Ravindran, 2010; Ogunsua et al. 2014; Rabiu et al. 2015; Papadimitriou et al. 2020; Oludehinwa et al. 2021). Based on the dynamical nature of the ionosphere, the occurrence of TIDs possesses some dynamical characteristics that need to be unveil by determining the degree of dynamical complexity response in the dynamics of the ionosphere. Interestingly, the distribution of dynamical complexity response in the day-to-day ionospheric dynamics was evidently depicted in all the stations. It was found that the degree of dynamical complexity responses reduces, as the propagation of TIDs signatures begins to emerge. As the signatures of the TIDs begins to subsides, the degree of dynamical complexity response increases. The features of dynamical complexity distribution revealed that the propagation of traveling ionospheric disturbances in the Eastern Africa sector spreads from the Southern Hemisphere (SH) and diminishes at the Northern Hemisphere (NH). Notably, the response of dynamical complexity at ADIS and NEGE was high and the stations situated within the southern Hemisphere depicts low degree of dynamical complexity response. These observed dynamical complexity response signifies that the propagation of TIDs in the Southern Hemisphere is more pronounced compared to the Northern Hemisphere. Its further implies that the propagation of TIDs due to the 2015 major geomagnetic storms in ADIS and NEGE is minimal.

Most of the day-to-day observation of dynamical complexity response in March 2015 depicts low values signifying that the occurrence of TIDs due to March 2015 geomagnetic activities is highly pronounced. These observations of reduction in dynamical complexity response during

398 the March 2015 may be attributed to Equinoctial factor. During the equinoctial and summer
399 months, the ionospheric system is induced by the Equatorial Ionospheric Anomaly (EIA); in that,
400 the daytime (nighttime) F region plasma is transported by a vertical upward (downward) $E \times B$
401 drift, created by interaction between the ionospheric electric-field and the geomagnetic B field
402 over the dip equator, and by field-aligned diffusion on both sides of the dip equator. These
403 processes have a tendency to create a plasma distribution symmetric to the dip equator and local
404 TEC gradient (Maruyama et al. 2005; Horvath and Lovell, 2010; Spogli et al., 2003; Bolaji et al.,
405 2022).

406 Comparatively, in June 2015, the degree of dynamical complexity distribution was generally
407 high when compared to March 2015 geomagnetic storm. High degree of dynamical complexity
408 response at ADIS and NEGE were also observed which further strengthening the evidence that
409 the occurrence of TIDs at ADIS and NEGE is minimal. Reduction in dynamical complexity
410 found at MOIU, DODM, and MBEY signifies that the occurrence of TIDs is significant during
411 June 2015 geomagnetic storm. During December 2015 geomagnetic storm, the day-to-day
412 dynamical complexity response was higher compared to June and March major geomagnetic
413 storms. These observed features of dynamical complexity response in June and December, 2015
414 signifies that the propagation of TIDs is nominal in the month of June and December. Notably,
415 the month of June and December are solstitial month. Therefore, the propagation of TIDs is more
416 prominent at Equinoctial season compared to solstitial season.

417 The latitudinal observation of TIDs during different phases of March 2015 major geomagnetic
418 storm depicts low degree of dynamical complexity at initial, main and recovery phases. The
419 lowest degree of dynamical complexity was observed during the initial and recovery phases. This
420 observation implies that the propagation of TIDs is driven at all the phases of geomagnetic

storm. We suspect that the influence of magnetospheric-ionospheric coupling processes and meteorological factors could be responsible for the generation of TIDs occurrence at initial and recovery phases of geomagnetic storm (Meng et al. 2019a; Borchevkina et al. 2021).

In June 2015 geomagnetic storm, high degree of dynamical complexity distribution was observed during all the phases. However, at main and recovery phases slight reduction in dynamical complexity was noticed. Similar features of dynamical complexity distribution were also found during December 2015 geomagnetic storm. Notably, the response of dynamical complexity in December 2015 is higher at all the phases compared to June and march 2015 geomagnetic storm.

5.0 Conclusion

This study had applied Neural Network Entropy (NNetEn) to examine the nonlinear dynamical characteristics associated with the occurrence of TIDs during 2015 major geomagnetic storms. Eight GPS stations situated within the Eastern Africa sector was investigated. Neural Network Entropy (NNetEn) which measures the degree of dynamical complexity was applied to the

detrended TEC time series data to capture the dynamical characteristic associated with TIDs occurrence. The results of the NNetEn were able to track distinct features associated with TIDs occurrence such that reductions in the degree of dynamical complexity responses were associated with the emergence of TIDs while increments in the response of dynamical complexity was observed during the absence of TIDs. ADIS and NEGE depicts high degree of dynamical complexity response in the day-to-day NNetEn observation signifying the development of TIDs at ADIS and NEGE is minimal. It was also observed that reduction in dynamical complexity response associated with the emergence of TIDs is more evident in the Southern Hemisphere compared to Northern Hemisphere indicating that the development of TIDs is more pronounced in the Southern Hemisphere. Interestingly, we further found that the response of dynamical complexity associated with TIDs features expands from the Southern Hemisphere and diminishes at the Northern Hemisphere. Furthermore, we found that the propagation of TIDs is more prominent at Equinoctial season compared to solstitial season. Finally, the reduction in dynamical complexity associated with the occurrence of TIDs were obvious during all the phases of geomagnetic storms. In particular, the initial and recovery phases of geomagnetic storm depict dynamical complexity response associated with TIDs occurrence.

Acknowledgements

The authors would like to acknowledge the World Data Centre for Geomagnetism, Kyoto, Japan, the National Aeronautics and Space Administration (NASA), Space Physics Facility and the International Services of geomagnetic Indices (ISGI) for making available the near-Earth

magnetic field data. We also appreciate the efforts of UNAVCO (https://www.unavco.org) for providing GPS/GNSS Data for research purpose. The Neural Network Entropy (NNetEn) software is free available from the website (https://www.mdpi.com/article/10.3390/e23111432/s1)

References

Adebesin, B. O., Rabiu, A. B., Bolaji, O. S., Adeniyi, J. O., Amory-Mazaudier, C. (2018). Ionospheric climatology at Africa EIA trough stations during descending phase of sunspot

cycle 22. Journal of Atmospheric and Solar-Terrestrial Physics, 172, 88-99. https://doi.org/10.1016/j.jastp.2018.03.009

Altadill, D., Segarra, A., Blanch, E., Juan, J. M., Paznukhov, V. V., Buresova, D., Belehaki, A. (2020). A method for real-time identification and tracking of traveling ionospheric disturbances using ionosonde data: first results. Journal of Space Weather and Space Climate, 10, 2. doi:10.1051/swsc/2019042

Amaechi, P. O., Oyeyemi, E. O., Akala, A. O. (2018). The response of African equatorial/low-latitude ionosphere to 2015 St. Patrick's Day geomagnetic storm. Space Weather, 16, 601–618. https://doi.org/10.1029/2017SW001751.

Arowolo, O. A., Akala, A. O., Oyeyemi, E. O. (2020). Interplanetary origins of some intense geomagnetic storms during Solar Cycle 24 and the responses of African equatorial/low latitude ionosphere to them. Journal of Geophysical Research: Space Physics, 126, e2020JA027929. https://doi.org/10.1029/2020JA027929.

Artru, J., Ducic, V., Kanamori, H., Lognonné, P., Murakami, M. (2005). Ionospheric detection of gravity waves induced by tsunamis. Geophysical Journal International, 160, 840–848. doi: 10.1111/j.1365-246X.2005.02552.x

Azeem, I., Vadas, S. L., Crowley, G., Makela, J. J. (2017). Traveling ionospheric disturbances over the United States induced by gravity waves from the 2011 Tohoku tsunami and comparison with gravity wave dissipative theory. Journal of Geophysical Research: Space Physics, 122, 3430–3447. https://doi.org/10.1002/2016JA023659

503 Balasis, G., Papadimitriou, C., Boutsi A. Z., (2019). Ionospheric response to solar and
504 interplanetary disturbances: a Swarm perspective. Phil. Trans. R. Soc. A 377: 20180098.
505 http://dx.doi.org/10.1098/rsta.2018.0098

506 Bolaji, O.S., Adekoya, B. J., Adebiyi, S. J., Adebesin, B. O., Ikubanni, S. O. (2022). The African
507 Equatorial Ionization Anomaly response to the St. Patrick's Day Storms of March 2013 and
508 2015. Astrophys Space Sci., 367(1). doi: 10.1007/s10509-021-04022-5

509 Borchevkina, O. P., Kurdyaeva, Y. A., Dyakov, Y. A., Karpov, I. V., Golubkov, G. V., Wang, P.
510 K., Golubkov, M. G. (2021). Disturbances of thermosphere and the ionosphere during a
511 Meteorological storm. *Atmosphere*, 12, 1384, doi: 10.3390/atmos12111384.

512 Bromba, M. U. A., & Ziegler, H. (1981). Application hints for Savitzky-Golay digital smoothing
513 filters. Analytical Chemistry, 53(11), 1583–1586. doi:10.1021/ac00234a011

514 Burleigh, M. R., Heale, C. J., Zettergren, M. D., Snively, J. B. (2018). Modulation of low-
515 altitude ionospheric upflow by linear and nonlinear atmospheric gravity waves. Journal of
516 Geophysical Research: Space Physics, 123, 7650–7667.
517 https://doi.org/10.1029/2018JA025721

518 Cheng, P., Lin, C., Yuichi Otsuka, Y., Liu, H., Rajesh, P.K., Chen, C., Jia-Ting Lin, J., M. T.
519 Chang, M. T., (2021). Statistical study of medium-scale traveling ionospheric disturbances
520 in low-latitude ionosphere using an automatic algorithm. Earth, Planets and Space (2021)
521 73:105 https://doi.org/10.1186/s40623-021-01432-1

522 Cherniak, I., Zakharenkova, I. (2018). Large-scale traveling ionospheric disturbances origin and
523 propagation: Case study of the December 2015 geomagnetic storm. Space Weather, 16,
524 1377–1395. https://doi.org/10.1029/2018SW001869.

Ciraolo, L., Azpilicueta, F., Brunini, C., Meza, A., and Radicella, S. M. (2007). Calibration Errors on Experimental Slant Total Electron Content (TEC) Determined with GPS. J. Geodesy 81, 111–120. doi:10.1007/s00190-006-0093-1

Ciraolo, L., Spalla, P., (1997). Comparison of ionospheric total electron content from the navy navigation satellite system and the GPS. Radio Sci., 32(3), 1071-1080. https://doi.org/10.1029/97RS00425

de Jesus, R., Batista, I. S., Jonah, O. F., de Abreu, A. J., Fagundes, P. R., Venkatesh, K., Denardini, C. M. (2017). An investigation of the ionospheric disturbances due to the 2014 sudden stratospheric warming events over Brazilian sector. Journal of Geophysical Research: Space Physics, 122, 11,698–11,715. https://doi.org/10.1002/2017JA024560.

Dewar, R. E., Wallis, J. R. (1999). Geographical pattern of interannual rainfall variability in the tropics and near tropic: An L-moments Approach. Journal of Climate, 12, 3457-3466. https://doi.org/10.1175/1520-0442(1999)012<3457:GPOIRV>2.0.CO;2

Ding, F., Wan, W., Ning, B., Wang, M. (2007). Large-scale traveling ionospheric disturbances observed by GPS total electron content during the magnetic storm of 29-30 October 2003. Journal of Geophysical Research: Space Physics, 112(A6), 1-15. doi:10.1029/2006ja012013.

Fejer, B. G., Scherliess, L., de Paula, E. R. (1999). Effects of the vertical plasma drift velocity on the generation and evolution of equatorial spreadF. Journal of Geophysical Research: Space Physics, 104(A9), 19859–19869. doi:10.1029/1999ja900271

Ferreira, A. A., Borries, C., Xiong, C., Borges, R. A., Mielich, J., & Kouba, D. (2020). Identification of potential precursors for the occurrence of Large-Scale Traveling

Ionospheric Disturbances in a case study during September 2017. Journal of Space Weather and Space Climate, 10, 32. doi:10.1051/swsc/2020029

Freeshah, M., Zhang, X., Chen, J., Zhao, Z., Osama, N., Sadek, M., Twumasi, N. (2020). Detecting ionospheric TEC disturbances by three methods of detrending through dense CORs during a strong thunderstorm. Annals of Geophysics, 6(63), 1-19, doi: 10.4401/ag-8372

Fuller-Rowell, T. J., Codrescu, M. V., Rishbeth, H., Moffett, R. J., Quegan, S. (1996). On the seasonal response of the thermosphere and ionosphere to geomagnetic storms. Journal of Geophysical Research: Space Physics, 101(A2), 2343–2353. doi:10.1029/95ja01614

Habarulema, J. B., Katamzi, Z. T., & Yizengaw, E. (2015), First observations of poleward large-scale traveling ionospheric disturbances over the African sector during geomagnetic storm conditions, J. Geophys. Res. Space Physics, 120, 6914–6929, doi:10.1002/2015JA021066.

Hocke, K., Schlegel, K. (1996). A review of atmospheric gravity waves and traveling ionospheric disturbances: 1982–1995. Annales denGeophysique, 14, 917–940. https://doi.org/10.1007/s00585-996-0917-6

Horvath, I., Lovell, B. C. (2010). Traveling ionospheric disturbances and their relations to storm-enhanced density features and plasma density irregularities in the local evening and nighttime hours of the Halloween superstorms of 29-31 October 2003. Journal of Geophysical Research: Space Physics, 115(A9), 1-16. doi:10.1029/2009ja015125

Hunsucker, R. The sources of gravity waves. Nature 328**,** 204–205 (1987). https://doi.org/10.1038/328204a0

568 Imtiaz, N., Younas, W., & Khan, M. (2020). Response of the low- to mid-latitude ionosphere to
569 the geomagnetic storm of September 2017. Annales Geophysicae, 38(2), 359–372.
570 doi:10.5194/angeo-38-359-2020.

571 Jiang, C., et al. (2017), Equatorial and low-latitude ionospheric response to the 17–18 March
572 2015 great storm over Southeast Asia longitude sector, J. Geophys. Res. Space Physics,
573 122, 5756–5767, doi:10.1002/2017JA024134.

574 Jonah, O.F., Zhang, S., Coster, A.J., Goncharenko, L.P., Erickson, P.J., Rideout, W., de Paula,
575 E.R., de Jesus, R. (2020). Understanding Inter-Hemispheric Traveling Ionospheric
576 Disturbances and Their Mechanisms. Remote Sens., 12, 228.
577 https://doi.org/10.3390/rs12020228

578 Joseph, O. O., Yamazak, Y., Cilliers, P., Baki, P., Ngwira, C. M., Mito, C. (2015). A study on
579 the response of the Equatorial Ionization Anomaly over the East Africa sector during the
580 geomagnetic storm of November 13, 2012. Advances in Space Research, 55(12), 2863–
581 2872. doi: 10.1016/j.asr.2015.03.011

582 Kelley, M. C., Makela, J. J., Chau, J. L., Nicolls, M. J. (2003). Penetration of the solar wind
583 electric field into the magnetosphere/ionosphere system, Geophys. Res. Lett., 30 (4), 1158,
584 doi:10.1029/2002GL016321, 2003.

585 Kelley, M.C. (1989) The Earth's Ionosphere, Plasma Physics and Electrodynamics. Academic
586 Press, Inc., San Diego, California.

587 Kelley, M.C., J.J. Makela, J.L. Chau, and M.J. Nicolls, (2013). Penetration of the solar wind
588 electric field into the magnetosphere/ionosphere system, Geophys. Res. Lett., 30 (4), 1158,
589 https://doi.org/10.1029/2002GL016321

590 Keskinen, M.J., Szuszczewicz, E.P., S.L. Ossakow, E.P., J.C. Holmes, E.P. (1981). Nonlinear
591 theory and experimental observations of the local collisional Rayleigh-Taylor instability in
592 a descending equatorial spread F ionosphere, J. Geophys. Res., 86 (A7), 5785, 1981.

593 Kundu, B., Senapati, B., Matsushita, A., Heki, K. (2021). Atmospheric wave energy of the 2020
594 August 4 explosion in Beirut, Lebanon, from ionospheric disturbances. Scientific Reports,
595 11(1). doi:10.1038/s41598-021-82355-5

596 Liu, J., Zhang, D.-H., Coster, A. J., Zhang, S.-R., Ma, G.-Y., Hao, Y.-Q., Xiao, Z., (2019). A
597 case study of the large-scale traveling ionospheric disturbances in the eastern Asian sector
598 during the 2015 St. Patrick's Day geomagnetic storm, Ann. Geophys., 37, 673–687,
599 https://doi.org/10.5194/angeo-37-673-2019.

600 Ma, G., Li, Q., Li, J., Wan, Q., Fan, J., Wang, X., … Zhang, J. (2020). A study of ionospheric
601 irregularities with spatial fluctuation of TEC. Journal of Atmospheric and Solar-Terrestrial
602 Physics, 211, 105485. doi: 10.1016/j.jastp.2020.105485

603 Maletckii, B., Astafyeva, E. (2021). Determining spatio-temporal charateristics of coseismic
604 travelling ionospheric disturbances (CTID) in near real-time. Scientific Reports., (2021)
605 11:20783. https://doi.org/10.1038/s41598-021-99906-5

606 Mañé, R., (1981). On the dimension of the compact invariant sets of certain nonlinear maps, in:
607 Dynamical Systems and Turbulence, editd by: Rand, D. and Young, L. S., Warwick 1980,
608 Springer, Berlin, Heidelberg, Lecture Notes in Mathematics, 898, 230– 242,
609 https://doi.org/10.1007/BFb0091916.

610 Maruyama, N., Richmond, A. D., Fuller-Rowell, T. J., Codrescu, M. V., Sazykin, S., Toffoletto,
611 F. R., Spiro, R. W., Millward, G. H. (2005). Interaction between direct penetration and

disturbance dynamo electric fields in the storm-time equatorial ionosphere. Geophysical Research Letters, 32(17). doi:10.1029/2005gl023763

Marwan, N., Romano, M.C., Thiel, M., Kurths, J., 2007. Recurrence plots for the analysis of complex systems. Phys. Rep. 2007, 237–329. https://doi.org/10.1016/J.physrep.2006.11.001, www.elsevier.com/locate/physrep.

Meng, X., Tsurutani, B. T., Mannucci, A. J., (2019a) The solar and interplanetary causes of superstorms (minimum Dst ≤ 250 nT) during the space age, J. Geophys. Res.-Space, 124, 3926–3948, https://doi.org/10.1029/2018JA026425.

Meng, X., Vergados, P., Komjathy, A., Verkhoglyadova, O. (2019b). Upper atmospheric responses to surface disturbances: An observational perspective. Radio Science, 54. https://doi.org/10.1029/2019rs006858

Mohannakumar, K. (2008). Stratosphere troposphere interaction: An introduction. Cochin, India: Springer.

Nade, D.P., Shetti, D.J., Sharma, A.K., Taori, A., Chavan, G.A., Patil, P.T. (2015). Geographical analysis of equatorial plasma bubbles by GPS and nightglow measurements. Adv. Space Res. 56(9), 1901–1910. https://doi.org/10.1016/j.asr.2015.03.030

Nishioka, M., Tsugawa, T., Kubota, M., Ishii, M. (2013). Concentric waves and short-period oscillations observed in the ionosphere after the 2013 Moore EF5 tornado. Geophysical Research Letters, 40(21), 5581–5586. doi:10.1002/2013gl057963

Occhipinti, G., Rolland, L., Lognonné, P., Watada, S. (2013). From Sumatra 2004 to Tohoku-Oki 2011: The systematic GPS detection of the ionospheric signature induced by

tsunamigenic earthquakes. Journal of Geophysical Research: Space Physics, 118(6), 3626–3636. doi:10.1002/jgra.50322

Odeyemi, O.O., Adeniyi, J.O., Oyeyemi, E.O., Panda, S.K., Jamjareegulgarn, P., Olugbon, B., Oluwadare, E. J., Akala, A. O., Olawepo, A.O., Adewale, A. A. (2022). Morphologies of ionospheric-equivalent slab-thickness and scale height over equatorial latitude in Africa, Advances in Space Research,69(1), 236-253. https://doi.org/10.1016/j.asr.2021.10.030.

Ogunsua, B. O., Laoye, J. A., Fuwape, I. A., & Rabiu, A. B. (2014). The comparative study of chaoticity and dynamical complexity of the low-latitude ionosphere, over Nigeria, during quiet and disturbed days. Nonlinear Processes in Geophysics, 21(1), 127–142. doi:10.5194/npg-21-127-2014

Ogunsua, B. O., Srivastava, A., Bian, J., Qie, X., Wang, D., Jiang, R., & Yang, J. (2020). Significant Day-time Ionospheric Perturbation by Thunderstorms along the West African and Congo Sector of Equatorial Region. Scientific Reports, 10(1). doi:10.1038/s41598-020-65315-3.

Oludehinwa, I. A., Olusola, O. I., Bolaji, O. S., and Odeyemi, O. O., (2018) Investigation of nonlinearity effect during storm time disturbance, Adv. Space. Res, 62, 440–456, https://doi.org/10.1016/j.asr.2018.04.032.

Oludehinwa, I. A., Olusola, O. I., Bolaji, O. S., Odeyemi, O. O., Njah, A. N. (2021). Magnetospheric chaos and dynamical complexity response during storm time disturbance. Nonlin. Processes Geophys., 28, 257-270, doi.org/10.5194/npg-28-257-2021.

Olwendo O. J, Baki, P., Cilliers, P. J., (2015). On the variability on the formation of Equatorial Ionization Anomaly crest over the East African low latitude region, 2015 1st URSI Atlantic

655 Radio Science Conference (URSI AT-RASC), 2015, 1-1, doi: 10.1109/URSI-AT-
656 RASC.2015.7303097.

657 Ostertagova, E., Ostertag, O., (2016) Methodology and Application of Savitzky-Golay Moving
658 Average Polynomial Smoother. Global Journal of Pure and Applied Mathematics. ISSN
659 0973-1768, 12(4), 3201-3210. www.ripublication.com/gjpam.htm

660 Oyedokun, O. J., Akala, A. O., Oyeyemi, E. O. (2020). Characterization of African Equatorial
661 Ionization Anomaly (EIA) during the maximum phase of solar cycle 24. Journal of
662 Geophysical Research: Space Physics. doi:10.1029/2019ja027066

663 Papadimitriou, C.; Balasis, G.; Boutsi, A.Z.; Daglis, I.A.; Giannakis, O.; Anastasiadis, A.;
664 Michelis, P.D.; Consolini, G. (2020). Dynamical Complexity of the 2015 St. Patrick's Day
665 Magnetic Storm at Swarm Altitudes Using Entropy Measures. Entropy 2020, 22, 574.
666 https://doi.org/10.3390/e22050574

667 Piek, A.B.; Stolz, I.; Keller, K. (2019). Algorithmics, Possibilities and Limits of Ordinal Pattern
668 Based Entropies. Entropy, 21, 547. https://doi.org/10.3390/e21060547

669 Pincus, S. M., (1991). Approximate entropy as a measure of system complexity, P. Natl. Acad.
670 Sci. USA, 88, 2297–2301, https://doi.org/10.1073/pnas.88.6.2297, 1991.

671 Rabiu, A. B., Ogunsua, B. O., Fuwape, I. A., Laoye, J. A. (2015). The transient variation in the
672 complexes of the low-latitude ionosphere within the equatorial ionization anomaly region
673 of Nigeria. Nonlinear Processes in Geophysics, 22(5), 527–543. doi:10.5194/npg-22-527-
674 2015

675 Richmond, A. D., Roble, R. G. (1979). Dynamic effects of aurora-generated gravity waves on
676 the mid-latitude ionosphere. Journal of Atmospheric and Terrestrial Physics, 41(7-8), 841–
677 852. doi:10.1016/0021-9169(79)90127-2

678 Savitzky, A., Golay, M. J. E. (1964). Smoothing and Differentiation of Data by Simplified Least
679 Squares Procedures. Analytical Chemistry, 36(8), 1627–1639. doi:10.1021/ac60214a047

680 Seba, E. B., Nigussie, M., Moldwin, M. B. (2018). The relationship between equatorial
681 ionization anomaly and nighttime equatorial spread F in East Africa. Advances in Space
682 Research, 62(7), 1737–1752. doi: 10.1016/j.asr.2018.06.029

683 Seemala, G.K., Valladares, C.E. (2011). Statistics of total electron content depletions observed
684 over the South American continent for the year 2008. Radio Sci. 46(5), 1-14.
685 https://doi.org/10.1029/2011rs004722

686 Seun, O. T., Jakowski, N., Valladares, C.E., Akala, A. O., Abe, O. E., Alizadeh, M. M., Schuh,
687 H. (2020). Climatology of Medium-Scale Traveling Ionospheric Disturbances (MSTIDs)
688 observed with GPS Networks in the North Africa Region. Research Square Preprint, doi:
689 10.21203/rs.3.rs-19043/v6

690 Shekhar, C. (2016). On simplified application of multidimensional Savitzky-Golay filters and
691 differentiators. AIP Conference Proceedings 1705, 020014. doi: 10.1063/1.4940262.

692 Sindelarova, T., Buresova, D., Chum, J., Hruska, F. (2009). Doppler observations of infrasonic
693 waves of meteorological origin at ionospheric heights. Advances in Space Research,
694 43(11), 1644–1651. doi: 10.1016/j.asr.2008.08.022

Song, Q., Ding, F., Wan, W., Ning, B., Liu, L., (2012). Global propagation features of large-scale traveling ionospheric disturbances during the magnetic storm of 7~ 10 November 2004. Annales Geophysicae 30 (4), 683–694. https://doi.org/10.5194/angeo-30-683-2012

Stauning, P., (2021) The Polar Cap (PC) index combination, PCC: relations to solar wind properties and global magnetic disturbances. J. Space Weather Space Clim., 11, 19, https://doi.org/10.1051/swsc/2020074.

Stubbe, P., Hagfors, T. (1997). The Earth's Ionosphere: A Wall-less Plasma Laboratory. Surveys in Geophysics 18, 57–127. doi.org/10.1023/A:1006583101811

Takens, F., (1981) Detecting Strange Attractors in Turbulence in Dynamical Systems, in: Dynamical systems and Turbulence, Warwick 1980. Lecture Notes in mathematics, Rand, D. and Young, L. S., Springer, Berlin, Heidelberg, vol. 898, https://doi.org/10.1007/BFb0091924.

Tsugawa, T. (2004). A statistical study of large-scale traveling ionospheric disturbances using the GPS network in Japan. Journal of Geophysical Research, 109(A6). doi:10.1029/2003ja010302

Tsurutani, B. T., Verkhoglyadova, O. P., Mannucci, A. J., Lakhina, G. S., Huba, J. D. (2012). Extreme changes in the dayside ionosphere during a Carrington-type magnetic storm. Journal of Space Weather and Space Climate, 2, A05. doi:10.1051/swsc/2012004

Tsurutani, B. T., Verkhoglyadova, O. P., Mannucci, A. J., Lakhina, G. S., Huba, J. D. (2012). Extreme changes in the dayside ionosphere during a Carrington-type magnetic storm. Journal of Space Weather and Space Climate, 2, A05. doi:10.1051/swsc/2012004

716 Unnikrishnan, K., Ravindran, S. (2010). A study on chaotic behaviour of equatorial/low latitude
717 ionosphere over Indian subcontinent, using GPS-TEC time series, Journal of Atmospheric
718 and Solar-Terrestrial Physics, 72 (14), 1080-1089,
719 https://doi.org/10.1016/j.jastp.2010.07.003

720 Unnikrishnan, K.S., Saito, A., Fukao, (2006). Differences in magnetic storms and quiet
721 ionospheric deterministic chaotic behaviour: GPS total electron content analyses. J.
722 Geophys. Res., 111, A06304, doi: 10.1029/2005JA011311.

723 Vadas, S. L., Crowley, G. (2017). Neutral wind and density perturbations in the thermosphere
724 created by gravity waves observed by the TIDDBIT sounder. Journal of Geophysical
725 Research: Space Physics, 122(6), 6652–6678. doi:10.1002/2016ja023828

726 Vadas, S. L., Liu, H. (2009). Generation of large-scale gravity waves and neutral winds in the
727 thermosphere from the dissipation of convectively generated gravity waves. Journal of
728 Geophysical Research: Space Physics, 114(A10), 1-25. doi:10.1029/2009ja014108.

729 Velichko, A. (2020). Neural Network for Low-Memory IoT Devices and MNIST Image
730 Recognition Using Kernels Based on Logistic Map. Electronics, 9(9), 1432.
731 doi:10.3390/electronics9091432

732 Velichko, A., Heidari, H. A., (2021). Method for Estimating the Entropy of Time Series Using
733 Artificial Neural Networks. Entropy, 23, 1432. https://doi.org/10.3390/e23111432.

734 Wen, Y. Jin, S. (2020). Traveling Ionospheric Disturbances Characteristics during the 2018
735 Typhoon Maria from GPS Observations. Remote Sens. 2020, 12, 746.
736 https://doi.org/10.3390/rs12040746

737 Yufei H, Zhao, X., Yang, D., Wu, Y., Li, Q., (2021). A study to investigate the relationship
738 between ionospheric disturbance and seismic activity based on Swarm satellite data,
739 Physics of the Earth and Planetary Interiors, 2021, 106826, ISSN 0031-9201,
740 https://doi.org/10.1016/j.pepi.2021.106826

741 Zhang, X., Tang, L. (2015). Detection of ionospheric disturbances driven by the 2014 Chile
742 tsunami using GPS total electron content in New Zealand, J. Geophys. Res. Space Physics,
743 120, 7918–7925, doi:10.1002/2014JA020879.

744 Zhu, X., Hu, Y., Zhao, Z., Ni, B., Zhang, Y. (2020). Ionospheric disturbance caused by artificial
745 plasma clouds under different release conditions. Earth Planets Space 72, 183.
746 doi.org/10.1186/s40623-020-01317-9

747

748

749

750

751

752

753

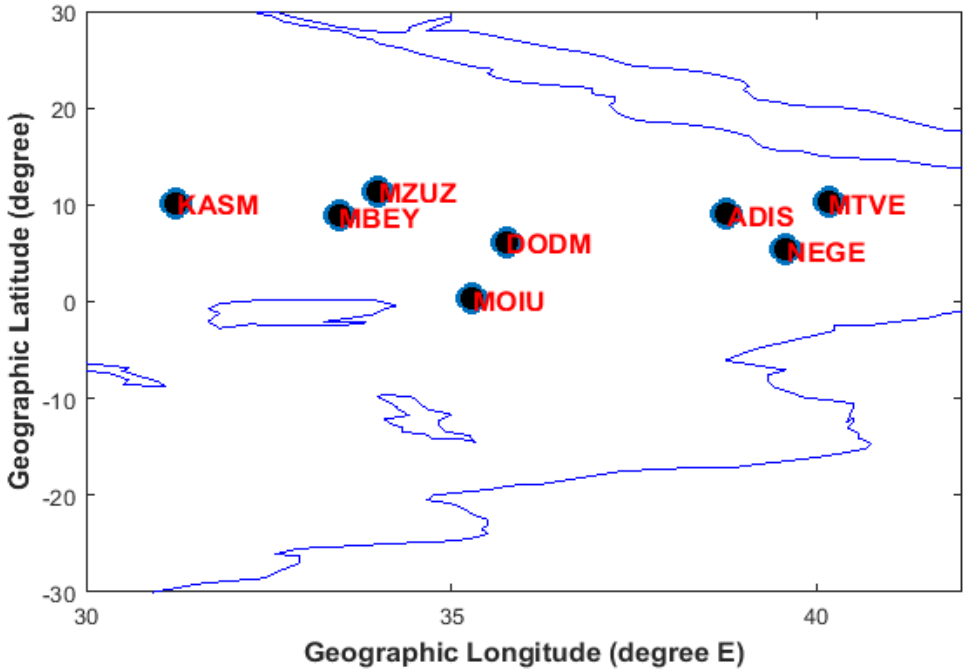

754

755 Figure 1: The geographical location of stations within the Eastern region of Africa sector

756

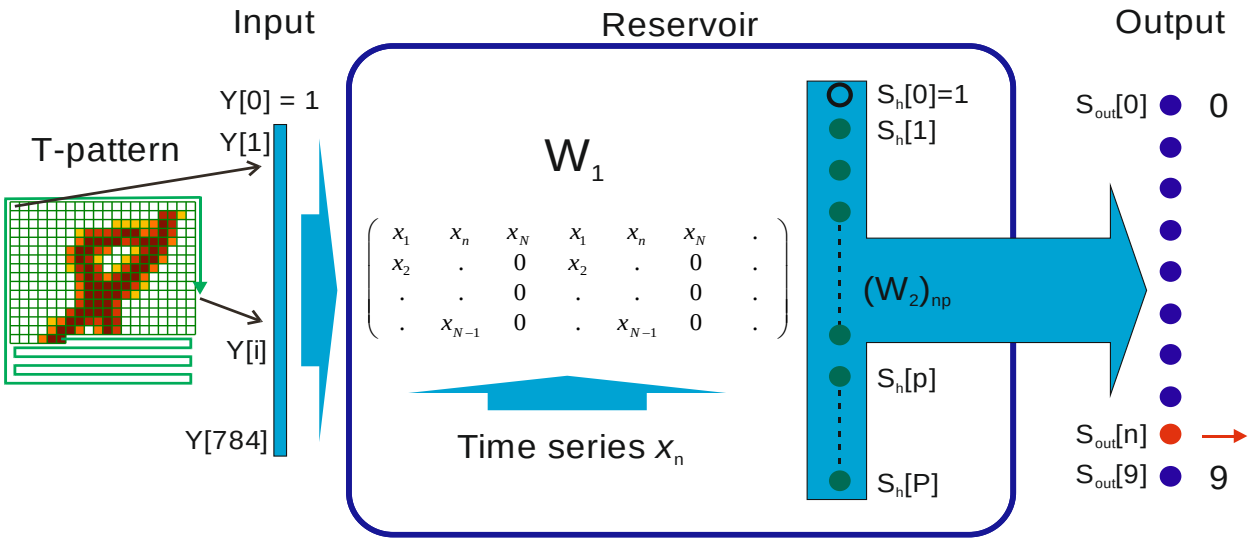

757

758 Figure 2: LogNNet model structure

759

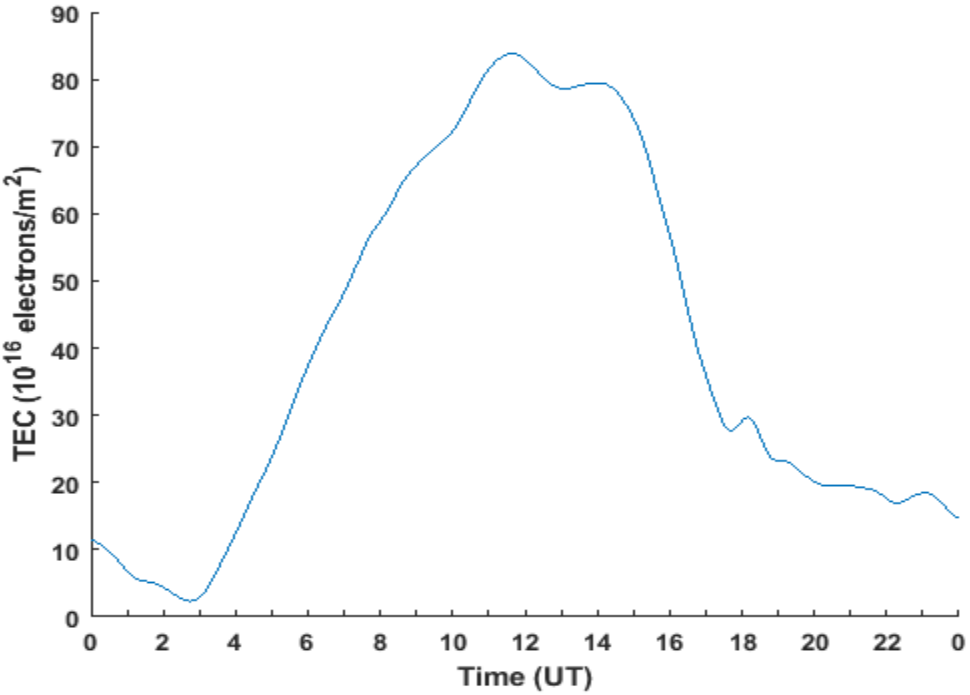

Figure 3: A sample of GPS-TEC time series measured at Addis Ababa on 26th March 2015.

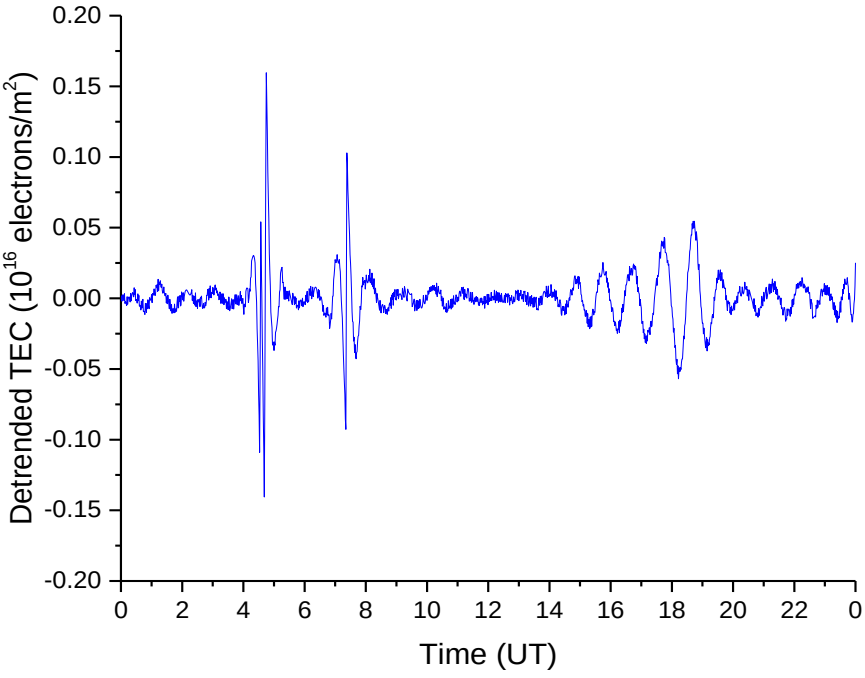

Figure 4: The detrended TEC depicting the presence of TIDs features at Addis Ababa on 26th March 2015.

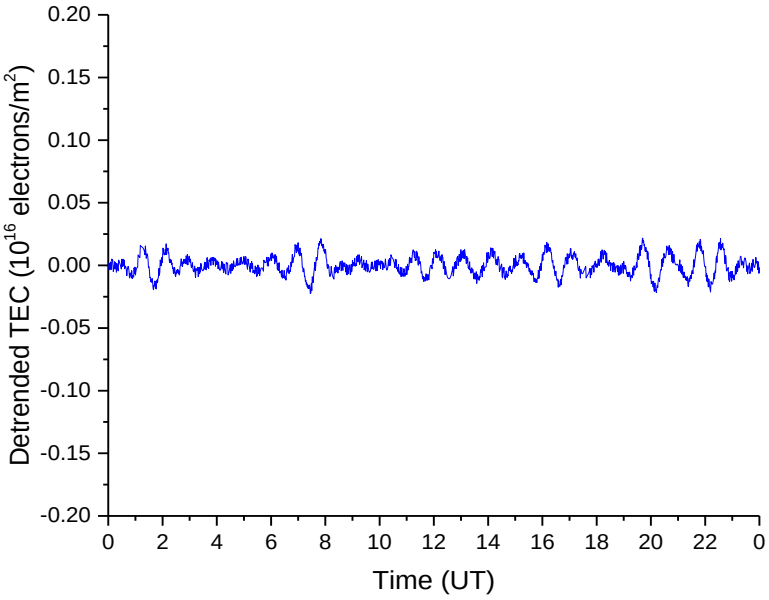

765

766 Figure 5: The time series data of detrended TEC depicting the absence of TIDs features at Addis

767 Ababa on 30th March 2015.

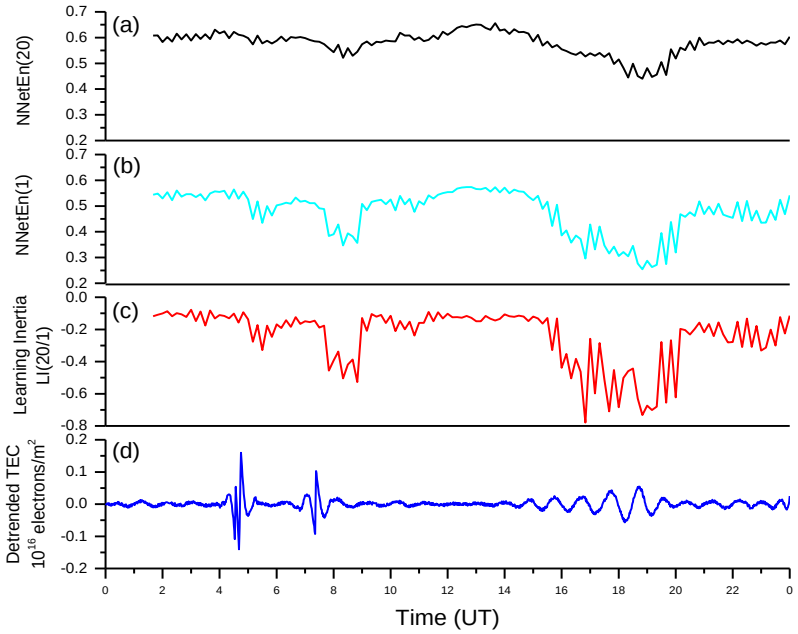

768

769 Figure 6: (a) NNetEn (20) (b) NNetEn (1) (c) Learning Inertia L1(20/1) (d) the time series of

770 detrended TEC depicting the presence of TIDs at Addis Ababa on 26th March 2015

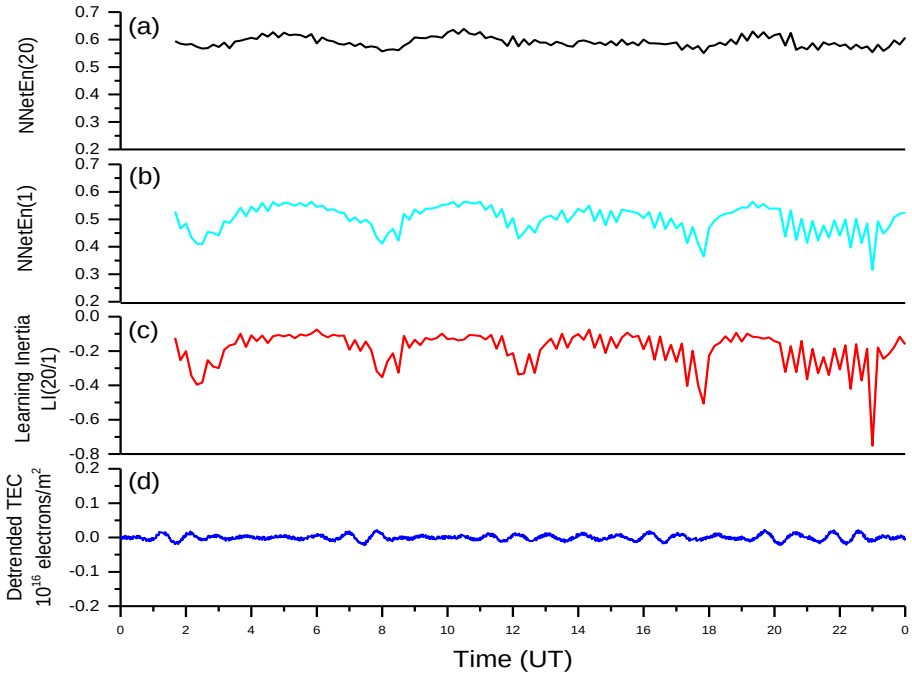

771

772 Figure 7: (a) NNetEn (20) (b) NNetEn (1) (c) Learning Inertia L1(20/1) (d) the time series of

773 detrended TEC depicting the absence of TIDs features at Addis Ababa on 30th March 2015

774

775

776

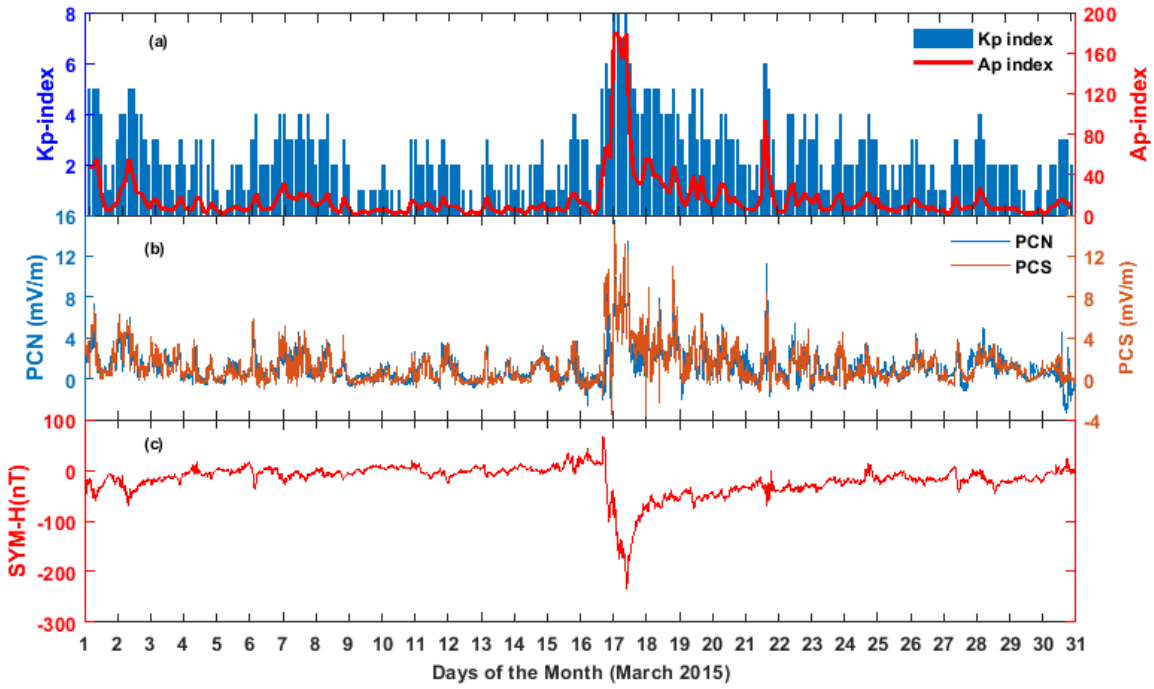

Figure 8: The global scale of geomagnetic activities during the month of March 2015 geomagnetic storm: (a) planetary indices Kp (in blue bar) and Ap (in red plot) (b) Polar Cap North index (PCN) in blue color and Polar Cap South index (PCS) in brown color (c) SYM-H

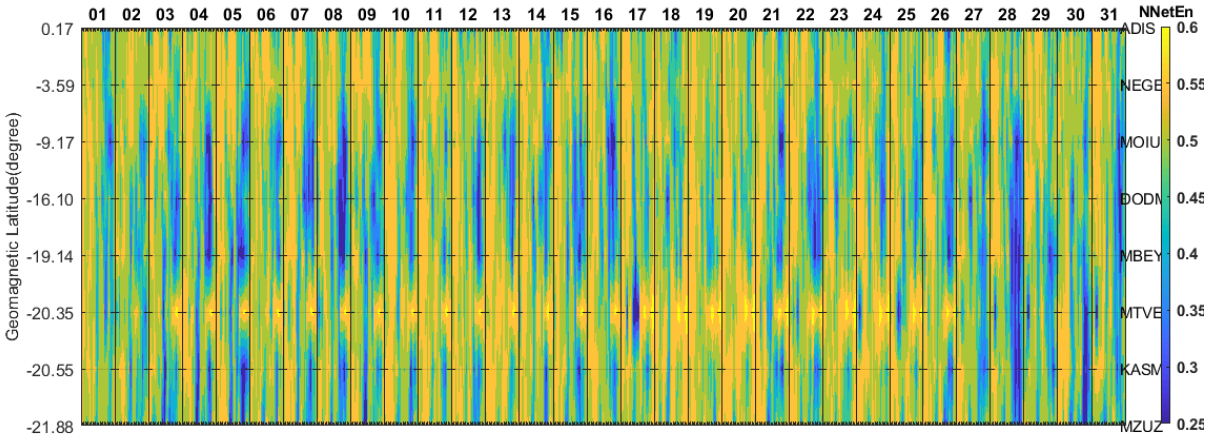

Figure 9: The Day-to-Day Latitudinal plot of NNetEn distribution across Eastern Africa during the March 2015 geomagnetic storm.

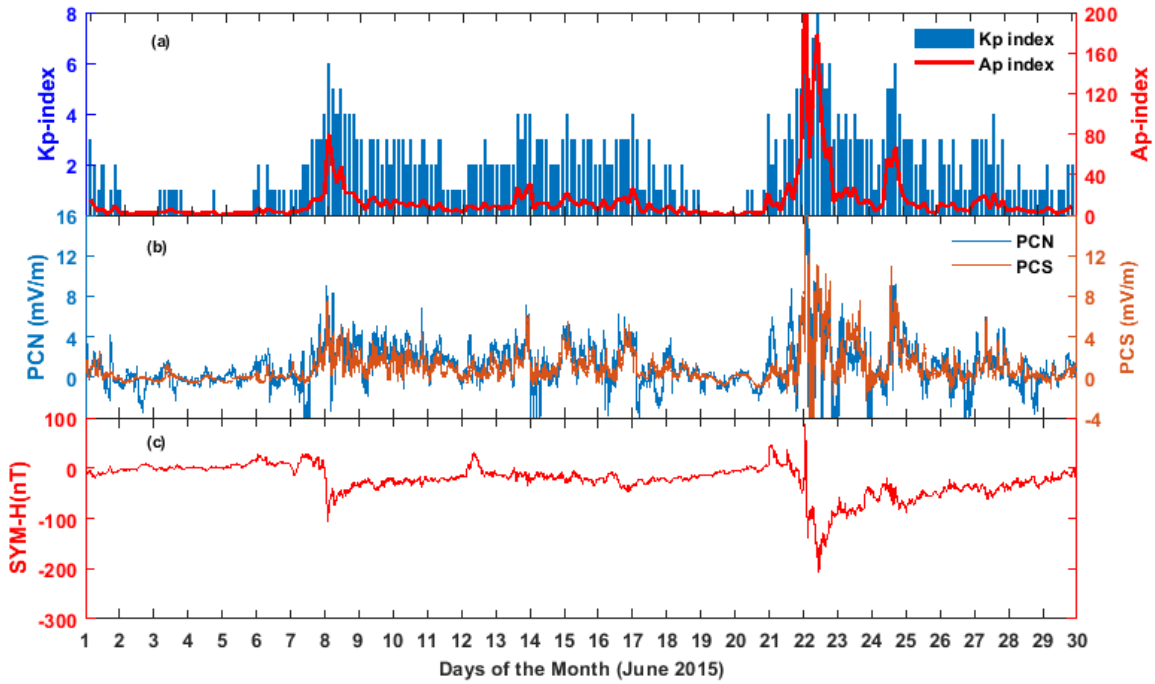

Figure 10: The global scale of geomagnetic activities during the month of June 2015 geomagnetic storm: (a) planetary indices Kp (in blue bar) and Ap (in red plot) (b) Polar Cap North index (PCN) in blue color and Polar Cap South index (PCS) in brown color (c) SYM-H

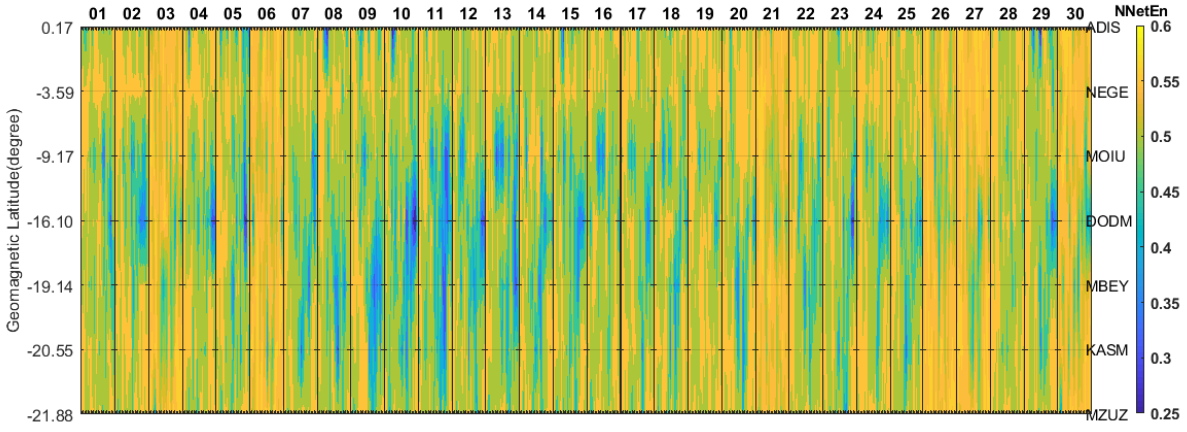

Figure 11: The Day-to-Day Latitudinal plot of NNetEn distribution across Eastern Africa during the June 2015 geomagnetic storm.

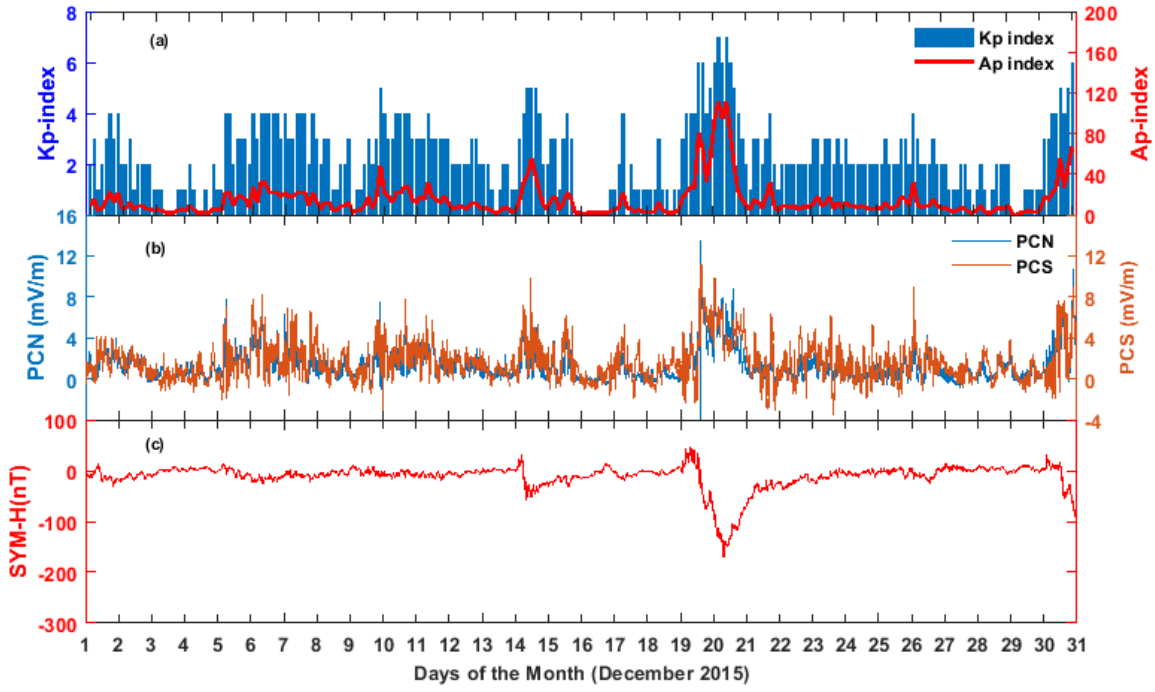

Figure 12: The global scale of geomagnetic activities during the month of December 2015 geomagnetic storm: (a) planetary indices Kp (in blue bar) and Ap (in red plot) (b) Polar Cap North index (PCN) in blue color and Polar Cap South index (PCS) in brown color (c) SYM-H

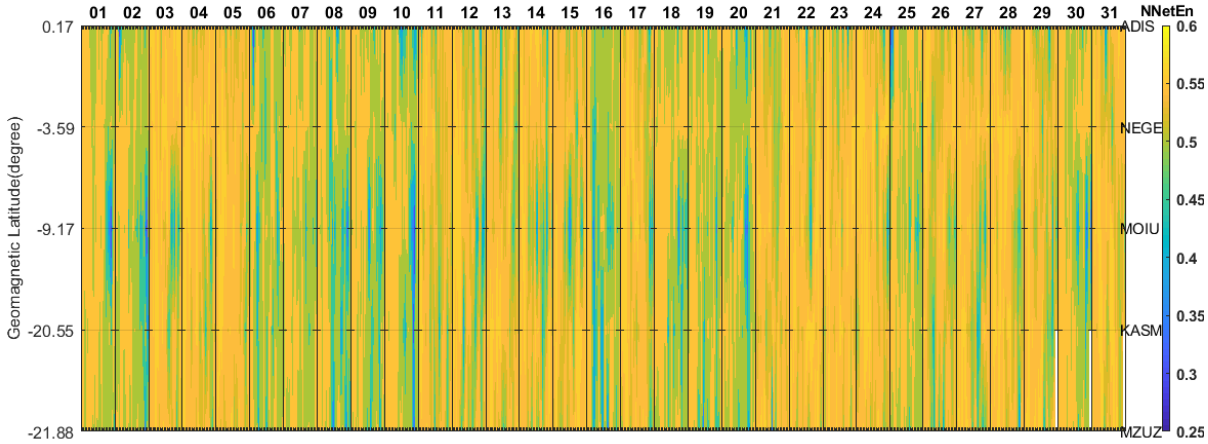

Figure 13: The Day-to-Day Latitudinal plot of NNetEn distribution across Eastern Africa during the December 2015 geomagnetic storm.

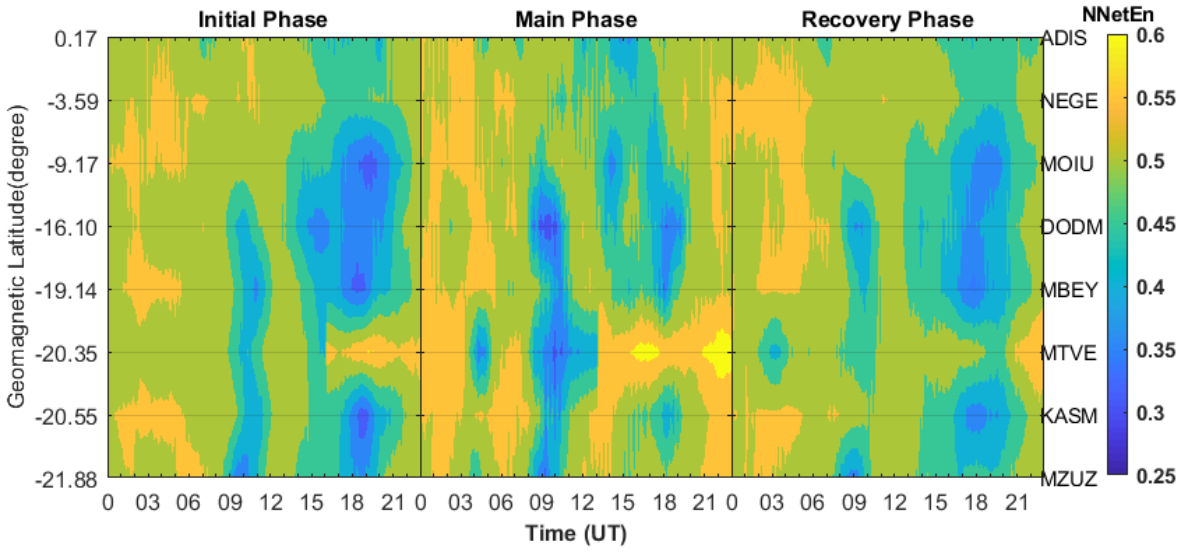

798

799 Figure 14: Latitudinal plot of NNetEn distribution at initial, main and recovery phases of March

800 2015 geomagnetic storm across the Eastern Africa.

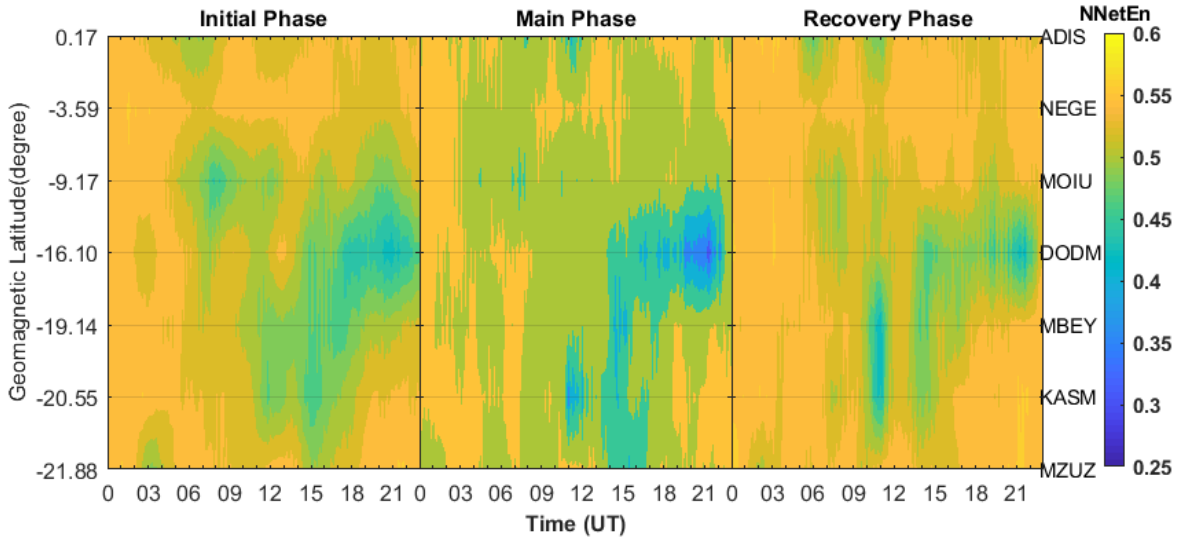

801

802 Figure 15: Latitudinal plot of NNetEn distribution at initial, main and recovery phases of June

803 2015 geomagnetic storm across Eastern Africa.

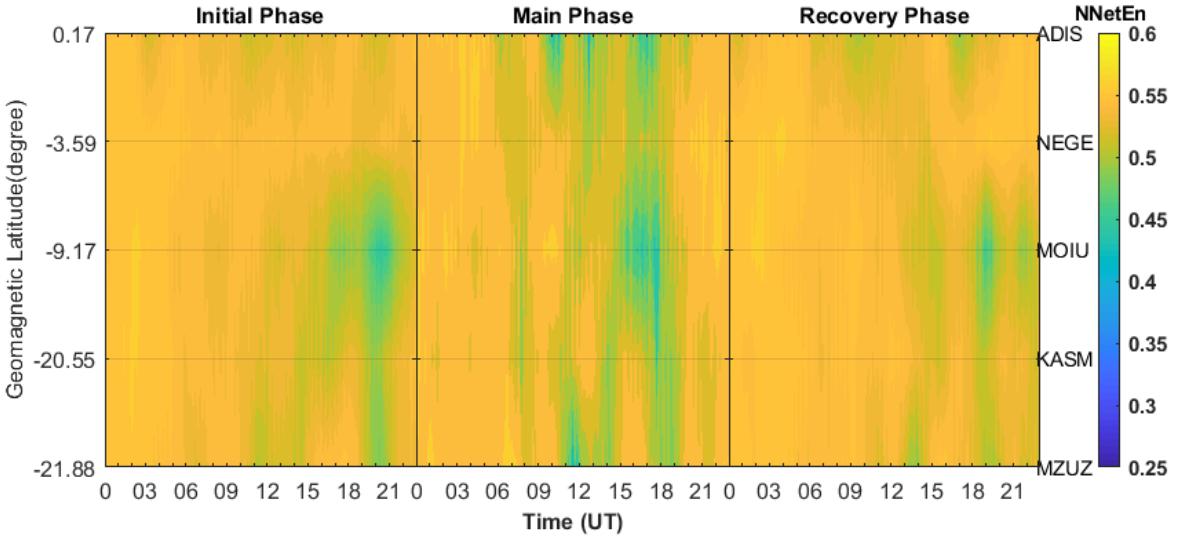

804

805 Figure 16: Latitudinal plot of NNetEn distribution at initial, main and recovery phases of

806 December 2015 geomagnetic storm across the Eastern Africa.

807

808

809

810

811

812

813

814

815

816

Table 1: The geographical and geomagnetic coordinates of stations investigated within Eastern region of Africa sector.

Stations Code	Country/State	Geographical Latitude	Coordinates Longitude	Geomagnetic Latitude	Coordinate Longitude
ADIS	Addis-Ababa, Ethiopia	9.0351^0N	38.7663^0E	0.17^0N	110.47^0E
NEGE	Negele, Ethiopia	5.3347^0N	39.5894^0E	-3.59^0N	111.36^0E
MOIU	Eldoret, Kenya	0.2883^0N	35.2900^0E	-9.17^0N	107.00^0E
DODM	Dodoma, Tanzania	6.1865^0S	35.7482^0E	-16.10^0S	107.21^0E
MBEY	Mbeya, Tanzania	8.9118^0S	33.4592^0E	-19.14^0S	104.66^0E
MTVE	Mtwara, Tanzania	10.2599^0S	40.1656^0E	-20.35^0S	111.24^0E
KASM	Misamfu, Zambia	10.1717^0S	31.2248^0E	-20.55^0S	102.24^0E
MZUZ	Mzuz, Malawi	11.4251^0S	34.0059^0E	-21.88^0S	104.92^0E

825